Screening for variable drug responses using human iPSC cohorts

Melpomeni Platani[1], Hao Jiang[1], Lindsay Davidson[2], Santosh Hariharan[3,4], Regis Doyonnas[3], Angus I. Lamond[1], Jason R. Swedlow[1] *

[1] Molecular Cell and Developmental Biology, School of Life Sciences, University of Dundee, Dow Street, Dundee DD1 5EH, Scotland, UK.

[2] Human Pluripotent Stem Cell Facility, School of Life Sciences, University of Dundee, Dow Street, Dundee DD1 5EH, Scotland, UK.

[3] Discovery Sciences, Pfizer, 445 Eastern Point Road, Groton, CT 06340, US Groton CT, USA.

[4] Current address: VRTX, 50 Northern Ave, Boston MA, 02210, USA.

* Corresponding author:

E-mail: jrswedlow@dundee.ac.uk

ABSTRACT

We have used a cohort of human induced pluripotent stem cell (hiPSC) lines to develop a laboratory-based drug screening platform to predict variable drug responses of potential clinical relevance. Our approach is based on the findings that hiPSC lines reflect the genetic identity of the donor and that pluripotent hiPSC lines express a broad repertoire of gene transcripts and proteins. We demonstrate that a cohort of hiPSC lines from different donors can be screened efficiently in their pluripotent state using high-throughput cell painting assays, allowing detection of variable phenotypic responses to a wide range of clinically approved drugs, across multiple disease areas. Furthermore, we provide information on mechanisms of drug-cell interactions underlying the observed variable responses by using quantitative proteomic analysis to compare sets of hiPSC lines that had been stratified objectively using cell painting data. We propose that information derived from comparative drug screening using curated libraries of hiPSC lines can help to increase the success rate of drug development pipelines and improve the delivery of safe new drugs suitable for a broad range of genetic backgrounds and gender diversity within human populations.

INTRODUCTION

Most current drug development pipelines involve an initial laboratory-based research phase, in which disease-relevant molecular targets are identified (usually proteins) and then either small molecules, or biological effectors (e.g. antibodies), are characterised that specifically bind to, or otherwise modulate, the targets. Promising drug candidates are then progressed to clinical trials, where they must be evaluated for efficacy and possible toxicity in human patients before they can be certified for use by regulatory authorities. Unfortunately, these pipelines often have very high failure rates, with 80% or more drug candidates in major disease areas failing to pass clinical trials (*1*). The high failure rates at late stages of drug development are a major factor in the high cost of bringing safe and effective new drugs to market.

A significant limitation with drug development pipelines is that they typically do not take into account effects that may disproportionately affect the suitability of drugs for use with patient groups from different sexes and/or genetic backgrounds. Variable drug responses resulting from natural variations in human biology have been cited as one of the major reasons for high failure rates of drug candidates in clinical trials (*2*). Fundamentally, drug development pipelines that map drugs to targets in the laboratory do not account for normal population-level differences between individuals.

There are now many examples of drugs used in oncology (*3*), anti-psychotics (*4*), cholesterol-lowering medications (*5, 6*) and others (*7*) where variable efficacy and toxicity are well-documented and included in standard dosing guidelines. In many cases, differential responses result from epistatic interactions and have been mapped to genetic variants affecting the expression levels and/or activity of, for example metabolic enzymes, other proteins acting in target pathways or membrane transporters. A key gap in the drug development pipeline, therefore, is the lack of assays that report on the impact of population-level phenotypic variation on drug-cell interactions during the pre-clinical phases of drug development.

Several projects have now established cohorts of human induced pluripotent cell (hiPSC) lines from multiple donors using standardised protocols (*8, 9*). In particular, the Human Induced Pluripotent Stem Cell Initiative (HipSci, https://www.hipsci.org), has established a library of >700 cell lines generated from over 300 individuals, including healthy male and female donors of varied ages, as well as patient cohorts with known genetic

disorders (*10*). The HipSci cell lines were all reprogrammed from human skin fibroblasts, following transduction of the pluripotency transcription factors using a Sendai virus vector (*10*). Many of these cell lines have been subjected to mRNA and protein expression analysis and all these data are publicly available. Interestingly, comparison of mRNA and protein expression patterns in the HipSci lines showed that mRNA and protein levels in separate hiPSC lines from the same individual are more similar to each other than to lines derived from different donors suggesting that the biomolecular states of th HipSci lines are strongy dfind by the genetic identity of the donor (*10, 11*). The HipSci cohort therefore provides a tractable system for measuring how human genetic variation affects cellular phenotypes, potentially including variable drug responses.

The ability of hiPSCs to be converted into defined cell types through standardised differentiation protocols is frequently used for experimental manipulation (*12*). However, the pluripotent state of hiPSCs provides a significant advantage for drug screening. Several studies have measured the range of gene transcript and protein expression in hiPSCs and embryonic stem cells (ESCs) (*11, 13*). In general, human ESCs and iPSCs express a broader repertoire of gene transcripts and proteins than terminally differentiated, primary cells and tissues, or in most tumour-derived transformed cell lines. For example, iPSC lines express ~2.5-fold more receptor tyrosine kinases than many primary cells or tumour cell lines. For the majority of chromosomes, >50% of their known protein coding genes are expressed in iPSCs ((*11*) and references therein). This broad molecular expression profile, including many pathways targeted by clinical therapeutics, makes the pluripotent state of hiPSCs an attractive foundation for compound and drug screening.

In this report, we describe the establishment and characterisation of a laboratory-based drug screening platform that compares drug responses between multiple hiPSC lines in the pluripotent state. The platform combines a cell painting assay advanced analytics and mass-spectrometry (MS)-based proteomic profiling to detect and explain variable drug responses. We validate the use of this screening platform using a wide variety of clinically-approved drugs that target diverse physiological pathways and disease areas.

RESULTS

Establishing Pluripotency in hiPSC Cohorts in High-Throughput Format

To test whether we could detect and characterize variable drug responses across a cohort of hiPSC lines from different donors, the high throughput cell painting assay (*14*) was first adapted to pluripotent hiPSC lines. We reasoned that we could use an image-based cell painting assay to detect variable responses and then employ quantitative MS-based proteomics to identify potential mechanisms causing variable response (see Figure 1A). We first established whether multiple hiPSC lines could be cultured in the pluripotent state in 384 multi-well plates, suitable for high content imaging and analysis. Twenty eight independent hiPSC lines derived from different donors (Suppl Table 1), were propagated in mTeSR medium, plated at $3x10^4$ cells/cm^2 in 384 multi-well plates for 72 hrs and then fixed and analysed by immunofluorescence to detect the established markers of pluripotency, i.e., Oct-4, Sox-2, Nanog and TRA-1-81 (Supp Figure 1A). All four markers showed strong, homogeneous staining.

We conclude, first, that multiple hiPSC lines can be cultured successfully in multi-well format suitable for large-scale, compound profiling by image analysis and second, that the panels of hiPSCs can be maintained in a pluripotent state throughout the 48-72 hours required for conducting the screening protocol.

Using Cell Painting to Profile Variable Drug Responses

Having characterised the growth conditions in 384 multi-well plates, the same set of 28 independent hiPSC lines from different donors (hereafter, “donors”) were grown in 384 multi-well plates for 24 hrs (see Methods for details), then treated either with a library of FDA-approved drugs, or with DMSO carrier, each at a single concentration (Suppl Table 2). After incubation for a further 24 hrs in the presence of the drugs, the cells were fixed and stained with cell painting markers (see Materials and Methods). Images were recorded in an automated, plate-based imager, then imported into OMERO (9). Images were segmented with respect to the ‘nuclei’, ‘cytoplasm’, ‘Golgi’ and ‘protrusions’, using a custom CellProfiler pipeline (*15*). For each drug-donor combination, image features were calculated, using 871 separate feature measurements from a total of 6,000-8,000 cells per donor-drug pair. After Robust Z’ normalisation, all measured features were

scaled as the number of standard deviations away from DMSO for each of the hiPSC lines (*14*).

Figure 1B shows a heatmap of the measured features of 28 donors, comparing treatment with 4 different drugs, i.e., atorvastatin, simvastatin, rapamycin and afatinib. The heatmap shows that each drug has characteristic feature patterns, but that different donors show varied magnitudes of response, visible as either darker, or lighter horizontal stripes, respectively (Figure 1B). The feature patterns for atorvastatin and simvastatin are similar, consistent with them having the same protein target, i.e., HMG CoA reductase. Interestingly, atorvastatin, which has a higher target affinity also shows a stronger response than simvastatin in this assay.

These data demonstrate that the cell painting assay, which was originally developed for analysis of immortalised cancer lines (*14*), also generates characteristic phenotypic fingerprints in hiPSC lines. Moreover, the data show that cell painting fingerprints from hiPSC cohorts reveal variable responses between the lines from different donors, with the major variation appearing as differences in the magnitude of features.

Next, the assay was expanded to profile the hiPSC cohort responses to 52 different FDA-approved drugs, which are used to treat a range of different diseases. To visualise this larger dataset, two different data reduction techniques were used because no single visualisation sufficed to reveal all relevant detail in this dataset. First, features were removed that had a Spearman correlation coefficient >0.98 which left 442 features for further analysis. The filtered features from all drug-donor pairs were then subjected to embedding with UMAP, which fits a manifold to a high-dimensional dataset and then projects this to a 2D plane (*16*) (Figure 2A). This showed that compound responses clustered according to their known mechanism of action. For example, statins, everolimus and rapamycin, topoisomerase inhibitors, cytotoxics and microtubule depolymerizers all formed separate, individual clusters. Interestingly, fluphenazine, an antipsychotic that acts by blocking specific dopamine receptors in the brain and that is used to treat schizophrenia and other psychotic disorders, clustered near the statins. This is consistent with reports that fluphenazine, like statins, affects lipid metabolism in human patients (*17*).

Besides showing that many drugs with similar modes of action cluster in this assay, the data also reveal cell lines that show variable responses to the same drugs. For example, when treated with rotenone, which disrupts microtubules, most hiPSC lines cluster together (“MT Modulators, Figure. 2A). An exception is the nufh4 cell line, which clusters

instead with hiPSC lines treated with fenbendazole. This is a drug which also causes microtubule depolymerisation, but by a different mechanism to rotenone, which mostly inhibits microtubule assembly dynamics (*18, 19*) (filled circles with trefoil, Figure 2A).

To test whether these results were reproducible, a selection of the previously analysed hiPSC lines were regrown from frozen stocks and analysed in cell painting assays after treatment with the same set of FDA-approved drugs, but this time using a different HCS imaging system (data collected on a Yokogawa CV7000 instead of InCell 2200). Using UMAP for visualisation, we observed that the cell painting features generated in this repeat set of assays were equivalent to those collected from the original experiment that was performed 6 months previously, using independent cultures of each hiPSC line and with data acquired using a different type of HCS imaging system (Suppl Figure 1B). We conclude that both the specific clustering responses of cell lines treated with different classes of drugs, as well as the variable responses observed to the same drug between cell lines derived from different donors, are reproducible in this assay format and represent intrinsic properties of the respective cell lines, independent of cell line stocks, prepared media or instrumentation used for image acquisition.

While many of the drug treatments resulted in tight clustering of the responses of different cell lines on the UMAP plots (Figure 2A), a subset of the drugs tested, i.e. statins, 5-FU, and erlotinib showed more dispersed clustering of cell line responses. We hypothesised that this behaviour reflected an increased degree of variable response to these drugs between the respective cell lines. To investigate potential mechanisms of variable response underlying clustering differences observed in UMAP plots, we next used linear approaches for measuring compound responses, aiming to avoid effects specific to clustering in high-dimensional spaces (*20*).

Figure 2B shows a heatmap of the cell painting induction, calculated as the fraction of filtered features > 2σ from DMSO (and thus significant with >95% certainty) (*21*). This has the effect of reducing the filtered features for each drug-donor pair to a single statistic and thus likely underestimates the complexity of phenotypes that give rise to clustering in UMAP. Nonetheless, this visualisation shows clearly that, first, hiPSC lines derived from different donors exhibit different levels of induction when treated with the same drugs and second, that examples of such differential response are observed between cell lines for all of the different drugs tested.

In all but one case, the individual cell lines show varied responses and appear to be either hyper- or hyposensitive to specific drugs. The exception was the cell line voce2,

which consistently showed a higher induction level (i.e., it is hypersensitive to most of the drugs used in this assay), than the other cell lines. Nonetheless, combining the results shown in Figure 1B (feature heatmap) and Figure 2B (induction heatmap), we conclude that a significant source of variable responses between donor cell lines seen in the cell painting assay results from differences in the magnitude of response shown by each line.

Linking Variable Responses to Protein Expression & Stoichiometry

Our previous studies on this HipSci cohort have demonstrated that variations in protein expression levels between lines derived from different donors can be controlled by specific genomic loci, i.e., protein Quantitative Trait Loci (pQTLs) (*11*). This suggested the hypothesis that a potential source of differential drug responses between hiPSC lines might be due to epistatic interactions, i.e., resulting from genomic variation between donors causing differences in protein expression that can modulate drug-induced phenotypes, for example by affecting the stoichiometry of components of drug response pathways (*22*). Importantly, this hypothesis takes into account drug-cell interactions outside of the direct interaction of a drug with its protein target. Furthermore, it can potentially explain why patterns of drug response features measured by cell painting appear similar across cell lines, while the magnitude of responses between lines differ, as seen in the feature and induction heatmaps (Figures 1B and 2B).

To test this hypothesis, we first used the induction plot (Figure 2B) and a graph of induction values (Supp Figure 1C), to classify cell lines as, respectively, “low” and “high” responders, for two well-characterised drugs, i.e., atorvastatin and simvastatin, that share the same target. Cell lines denw6 and zaie1 (“low responders”) and hayt1 and tuju1 (“high responders”), were each treated separately with either DMSO (control), or with either atorvastatin or simvastatin, each at 5 μM for 24 hrs, as in the cell painting assay. Following treatment, cell extracts were prepared and proteomes analysed by LC-MS/MS (see Methods). From the resulting data, differences in protein expression levels between DMSO- and drug-treated lines were visualised in ‘volcano plots’ (Figure 3). Combining data for treatment of all four cell lines with either atorvastatin (Figure 3A), or simvastatin (Figure 3B), showed that many of the proteins whose expression increased after drug treatment are involved in lipid metabolism (red dots in Figure 3A, B). Further, GO term enrichment analysis also showed a significant enrichment for expression of protein factors involved in lipid metabolism (Suppl Table 3 and 4). These data suggest that homeostatic mechanisms in the hiPSC lines respond to drug mediated inhibition of

cholesterol metabolism by increasing the expression of enzymes required for cholesterol synthesis. This result is consistent with what was observed in the cell painting assay, where all hiPSC lines assayed exhibited similar responses (Figure.2A).

While a common type of response to inhibition of cholesterol synthesis is seen across the hiPSC lines, differences were evident in the magnitude of responses between individual cell lines to atorvastatin, or simvastatin, as detected by cell painting induction (Figure 2B). We therefore tested whether such variation in response magnitude might be linked to differences in protein expression between the respective high and low response lines. Volcano plots comparing protein expression in the high and low response lines after treatment with either atorvastatin (Figure 4A), or simvastatin (Supp Figure. 2A), show that multiple proteins involved in the cholesterol synthesis pathway (highlighted in red), together with some other classes of proteins, have increased expression in the high response lines. These data are consistent with the hypothesis that differential protein expression may explain, at least in part, the differences in the magnitude of drug responses between individual hiPSC lines.

Next, we compared the expression of individual proteins in each of the four drug-treated lines. Proteins were identified whose expression differed significantly in high v low responders ($|\log_2 FC| > 0.263$). Figure 4B shows a heatmap comparing these protein expression differences. This reveals clear differences in the responses to the two statin drugs across the four cell lines, suggesting that there may be variation in the mechanisms of response to statin treatment between each hiPSC line (see also Supp Figure 2B).

Interestingly, changes in protein expression in the high response lines include increased expression of HMGCR and HMGCS1, which are directly involved in the cholesterol mevalonate synthesis pathway. In contrast, both “low response lines”, show increased expression of proteins involved in regulating the stability and recycling of lipoprotein receptor complexes, such as PCSK9, SCARB1, a cell surface HDL receptor that mediates HDL-cholesteryl ester uptake, as well as ApoE a plasma protein that participates in the transport of cholesterol and other lipids between cells and has been linked to the effect of statins (*23-31*). Lipoprotein receptor complexes play an important role in the regulation of plasma and intracellular cholesterol homeostasis (*32*). These differences in protein expression between the respective high and low responder hiPSC lines to statin treatment suggest that variable activity of biosynthetic and/or influx mechanisms may be involved in determining how each hiPSC line responds to statins.

In addition to identifying well-established targets of statins, using GO enrichment and STRING analysis (https://string-db.org/) to characterise the proteins whose expression increases in the high response lines identified factors involved in Rab protein signal transduction and in the metabolism of RNA (Figure 4C and Supp Figure 2C; Suppl Table 5 and 7), all of which are known to change expression upon statin treatment (*33-37*). In contrast, the low response lines showed increased expression of proteins linked to the actin cytoskeleton along with several ubiquitin E2 and E3 enzymes, suggesting that ubiquitin-conjugation levels may affect the degree of statin response (Figure 4D and Suppl Figure 2D; Suppl Table 6 and 8). These data support the view that there is a diversity of factors and pathways that can affect the cellular response to well-defined drug perturbations and these differences are due in part to their proteomic landscapes.

In summary, these data are consistent with the hypothesis that variable levels of response to statins, and potentially also to other classes of drugs, reflect population-level variations in gene and protein expression between the respective lines.

DISCUSSION

We have established the first laboratory pipeline for the systematic analysis of population-level variable drug responses, using a cohort of hiPSC lines, each derived from multiple, healthy donors (*10*). This pipeline provides a 'genetically-informed', high-throughput assay for identifying and characterising variable drug responses in human cells, using cell painting and quantitative proteomics.

The choice of screening hiPSC lines specifically in their undifferentiated, pluripotent state leverages the recent discovery that, at least in part, gene expression in hiPSC lines reflects the genetic identity of the donor at both the RNA and protein levels (*10, 11*). Thus, the undifferentiated hiPSC lines can behave as avatars of the donors, with respect to their proteomes and cellular phenotypes. The corollary is that by screening how panels of hiPSC lines from different donors respond to drug treatment in a standardised assay format, these lines can be stratified objectively based upon measurements of their varied phenotypic responses. We hypothesise that these data may reveal important information about variable human drug responses that is germane to clinically relevant differential drug responses between patients.

The data presented in this study show that features can be extracted from the analysis of high-throughput, cell painting, fluorescence microscopy images, and used to stratify differences in the magnitude of drug responses between different hiSPC lines, (illustrated in Figures 1 and 2). The data also show that the stratification of cell lines based upon their degree of drug response is reproducible in this assay format. Further, by using quantitative proteomic analysis to compare the stratified sets of hiPSC lines we show that additional information relevant to understanding the mechanisms underlying variable drug response phenotypes can be identified. We have focussed on proteome level analysis here because proteins are the direct targets of most drugs in clinical use and because proteins are also the primary mediators of most disease processes and mechanisms of drug action.

We propose a hypothesis to explain the reproducible, differential response to drug treatment that is detected between different hiPSC lines in the screening assay. This hypothesis postulates that variations between the cell lines, at the genomic and/or epigenomic level, in turn determine the respective proteomes and thereby lead to differences in drug-cell interactions. We envisage that drug-cell response phenotypes can reflect multiple epistatic interactions that are predominantly mediated at the proteome level. This hypothesis is supported by using mass spectrometry to compare

the proteomes of hiPSC lines that were stratified by cell painting as either 'high' or 'low' responders to treatment with either atorvastatin and simvastatin. While we have concentrated here on comparing protein expression levels between cell lines, we note that other comparative analyses, for example comparing protein phosphorylation and other protein post translational modifications (PTMs) and protein-protein interactions can also provide valuable insights into the mechanisms causing variable drug responses between the different cell lines.

In this study we have investigated potential mechanisms involved in the variable responses seen to statins in this screening assay. Statins are drugs developed to reduce the level of cholesterol in blood and thus lower the risk of developing cardiac and circulatory diseases, including angina, heart attack and stroke (*38*). Separate, but interconnected pathways control cholesterol homeostasis. Intracellular cholesterol homeostasis is governed both by cholesterol influx, mediated by lipoprotein receptors and by cholesterol synthesis, regulated by HMG-CoA reductase and the mevalonate pathway. Cholesterol efflux, mediated by transport proteins, is also important in preventing excessive accumulation of cholesterol inside cells. Each of these pathways respond to multiple inputs that collectively define cholesterol levels, including the modulation of protein stability by Ub-mediated proteolysis. Our data indicate that variable expression of multiple proteins involved in cholesterol homeostasis in the different hiPSC lines can affect the observed response to statin treatment. Even within the limited sample of different donor lines we have analysed so far, we see evidence of varied regulatory effects. Our comparative proteomic analysis supports the view that "high response" lines can be determined by modulation of the endogenous cholesterol synthesis pathway, while "low response lines" may instead reflect primarily regulation of the cholesterol influx and efflux pathways.

In conclusion, we have established and validated a flexible, laboratory-based high-throughput screening platform that can detect and characterise examples of variable drug response for clinically relevant therapeutics. We anticipate that the use of this platform can in future help to improve the success rate of clinical trials by predicting variable responses and providing evidence of biomarkers that may improve the selection of suitable patients most likely to benefit from new drug candidates. We also anticipate that the use of carefully selected hiPSC cohorts, derived from donors of different genders and genetic backgrounds, can help to improve the development of safe new drugs that are suitable for the needs of modern, diverse human societies.

Acknowledgements

We would like to thank members of the National Phenotypic Screening Centre and Human Pluripotent Stem Cell Facility at the University of Dundee for invaluable help and advice. We thank University of Dundee's School of Life Sciences for their support of this project.

Declaration of Conflicting Interest

The authors Melpomeni Platani, Angus I. Lamond, Jason R. Swedlow would like to declare a conflict of interest as founders of Tartan Cell Technologies, Ltd.

MATERIALS & METHODS

Cell Culture

Human iPSC lines used in this study were from the HipSci cohort as previously described (4). Feeder-free human iPSC lines were cultured in Essential 8 (E8) medium (E8 complete medium supplemented with (50x) E8 supplement ThermoFisher-A1517001) on tissue-culture dishes coated with 10 μg/cm^2 of reduced Growth Factor Basement Membrane matrix (Geltrex, ThermoFisher A1413202 resuspended in basal medium DMEM/F12 Thermo Fisher 21331020). Medium was changed daily.

To passage feeder-free hiPSC lines, cells were washed with PBS and incubated briefly (3-5 min), with 0.5 mM PBS-EDTA solution. The PBS-EDTA solution was removed, cell clusters were resuspended in E8 medium and seeded at ratios of 1:4 to 1:6, depending on their confluency, on Geltrex-coated tissue culture dishes. Once established, undifferentiated, feeder-free human iPSC lines were expanded and frozen, prior to transition to TeSR medium for further study. To transition to TeSR medium supplemented with bFGF (Peprotech 100-1813, at a final concentration of 30 ng/ml), Noggin (Peprotech 120-10C, at a final concentration of 10ng/ml), Activin A (Peprotech 120-14P, at a final concentration of 10ng/ml), E8 medium of hiPSC lines was exchanged daily with medium containing increasing amounts of TeSR medium, until human iPSC lines were completely maintained in TeSR medium alone. Length of time was variable typically 1-2 weeks.

To passage human iPSC lines transitioned to TeSR medium, cells were washed with PBS and incubated briefly with TrypLE Select (ThermoFisher 12563029), to create a single cell suspension prior to resuspension in TeSR medium supplemented with ROCK kinase inhibitor (Tocris 1254, at a final concentration of 10 μM), to enhance single cell survival, bFGF (Peprotech 100-1813, at a final concentration of 30 ng/ml), Noggin (Peprotech 120-10C, at a final concentration of 10ng/ml), Activin A (Peprotech 120-14P, at a final concentration of 10ng/ml) and seeded at a concentration of 5x10^4 cells/cm^2 on Geltrex-coated tissue culture dishes. 24 hrs after replating Rock kinase inhibitor was removed from the culture medium. Pluripotency of TeSR-transitioned hiPSC lines was verified by immunofluorescence (see below) prior to either cell banking, or experimental use. Cells were grown at 37°C and 5% CO_2. Medium was changed daily.

hiPSC line ID number and details of the cell lines are listed in Supp Table 1.

Cell Staining

384-well tissue culture plates (CellCarrier-384 Ultra Microplates, Perkin Elmer 6057300) were coated with human plasma fibronectin (Merck Millipore FC010) at a concentration of 5 µg/cm^2. Cells were passaged as described above with TrypLE Select, counted and seeded on the fibronectin-coated wells, at a concentration of 3x10^4 /cm^2. Cell line plating was in rows, with six wells per condition for each cell line. Cells were incubated for 24 hrs prior to drug treatment, followed by a further 24 hrs incubation before final fixation and staining and high content imaging. Antibody staining of a separate 384-well plate at 48 hrs confirmed that pluripotency was maintained at 48 hrs.

Mitotracker (Thermo Fisher M22426), staining was performed in live cells with a 30 min incubation at 37°C prior to fixation. Fixation, permeabilisation and immunostaining were performed at room temperature. 8% Paraformaldehyde in PBS (PFA, Sigma F8775), was added to an equal volume of cell culture medium in wells of a 384-well plate for a final concentration of 4% Paraformaldehyde and incubated for 15 min. Fixed cells were washed in PBS and permeabilised with 0.1% v/v Triton-X100 (Sigma) for 15 min. Following permeabilisation, cells were washed in TBS and stained with DAPI (Thermo Fisher D1306 at 5 µg/ml), SYTO 14 (Thermo Fisher S7576 at 2.5 µM), Concanavalin A (Thermo Fisher C11252 at 20 µg/ml), Phalloidin Alexa (Thermo Fisher A12381 at 66 nM), and WGA (Thermo Fisher W11262 at 11.8 µg/ml) for 1hr. Staining volume was 30 µl/well. Cell fixation, permeabilisation, staining and washing steps (2x, wash volume 50 µl) were performed using automated liquid handling systems (405 plate washer, BioTek–Tempest, Formulatrix).

Drug treatment

Drug dosing on 384-well plates was performed using an Echo acoustic liquid handler and corresponding software (Labcyte). Screened compounds were selected from the appropriate chemical library plates containing Cloud library (Enamine) and an in-house library of publicly available compounds. Drug dosing was performed at final concentrations of; etoposide 1.7 µM, Berberine Chloride 2.68 µM, Fenbendazole 3.34 µM. For all other compounds drug dosing was performed at a final concentration of 5 µM. Supp Table 2 lists the compounds and their final concentrations used in this study. For proteomics analysis drug treatments with simvastatin (Tocris 1965) and atorvastatin; (Selleckchem S5715) were performed in triplicate in 6-well plates at a final concentration of 5 µM for 24hrs.

Cell staining and analysis of pluripotency markers

All cell lines used in this study were quality controlled for pluripotency prior and during the HCS assays. All fixation, permeabilisation and immunostaining analyses were performed at room temperature, apart from primary antibody incubation, which was carried out at 4°C overnight. 8% Paraformaldehyde in PBS (PFA, Sigma F8775), was added to an equal volume of cell culture medium in wells of a 384- well plate for a final concentration of 4% Paraformaldehyde and incubated for 15 min. Fixed cells were washed twice in PBS and permeabilised with 0.5% v/v Triton-X100 (Sigma) for 10 min (apart from TRA1-81 staining). Following permeabilization cells were washed twice in PBS, then blocked in 10% normal donkey serum for 1 hr prior to antibody incubations. Pluripotency marker antibodies used in this study are listed as follows: Nanog, Oct4, Sox2, Tra-1-81 all at 1:500, (Oct4 (C30A3), Sox2 (D6D9), Nanog (D73G4), TRA181 (TRA-1-81) Cell Signalling StemLight Pluripotency Antibody Kit 9656). All affinity purified donkey secondary antibodies (either Alexa 488 or Alexa 594) were purchased from Jackson Immunoresearch Europe. Hoechst 33342 (Thermo Fisher) was used to stain DNA. Images of of cells (for each hiPSC line , 9 fields/well, 16 wells per pluripotency marker) stained with pluripotency marker antibodies were segmented on DAPI signal and integrated nuclear intensity of each marker was quantified using CellProfiler. Distributions of integrated intensities of all nuclear pluripotency markers were monotonic and correlated with integrated DAPI staining. All cell lines used in this study were quality controlled for pluripotency prior and during the HCS assays.

For each experiment 8 wells of each cell line were individually stained with pluripotency marker antibodies

Imaging

Imaging data were collected on an InCell 2200 high content imager, with a 20x/NA 0.45 Plan Fluor lens and a Quad2 multichroic mirror (GE, Issaquah, WA) or a CV7000 high content imager, with a 20x/0.45 lens at epifluorescence mode (Yokogawa).

Data Processing, Analysis and Visualization of Multiple Cell Lines

Raw images were imported into OMERO Plus (Glencoe Software, Inc., (*39*)) and then processed using a custom pipeline in CellProfiler (*14*), which segmented nuclei, cytoplasm, Golgi and cortical protrusions and calculated a range of defined features. All further steps were executed using the Pandas Python library (*40*). Features for each plate were normalised by the median of features in the DMSO control for that plate.

Features with a coefficient of variation >0.50 were removed from further analysis. We further removed all features with |Spearman coefficient| > 0.98. Z-normalised data were then visualised using Uniform Manifold Approximation and Projection (UMAP (*16*)). UMAP parameters were n_neighbours = 15, mindist = 0.01 and a cosine metric was used for scaling distance between points. GO enrichment analysis was carried out using WebGestalt (WEB-based Gene SeT AnaLysis Toolkit) (*41, 42*). Functional protein-protein interaction analysis was carried out using STRING-DB (*43*).

Proteomics sample preparation

To support parallel MS-based proteomics analysis in this screening platform in a 6-well plate format, we also tested whether the expression of pluripotency markers was maintained when hiPSC lines were plated at $5x10^4$ cells/cm^2 prior to any drug addition and cultured as previously described. This showed that strong, homogeneous expression of the four pluripotency markers was maintained at this higher density (not shown).

All hiPSCs samples were washed twice with 1x PBS on ice twice, then centrifuged at 300g to collect the cell pellets. 4% SDS lysis buffer (10 mM TCEP, 100 mM Tris-HCl, pH 7.4) was used to lyse the cells and extract proteins, with 1x Protease and Phosphatase Inhibitor (A32961, Thermo Fisher) added. 1 mL lysis buffer was added to the cell pellets. After 10 cycles of sonication, (30s on/off), using the Bioruptor® Pico, the protein samples were centrifuged at 20,000*xg* for 15 min. The supernatant proteins were denatured at 95° for 10 min, then alkylated with 40 mM IAA (Iodoacetamide), (final concentration), incubated in the dark at room temperature for 30 min. The protein concentration was measured using the EZQ™ Protein Quantitation Kit following the manufacturer's instructions.

500 ug proteins from each sample were further processed using the SP3 protocol, as described (*44*). In brief, protein samples were mixed with SP3 beads (1:10, protein:beads) and digested with LysC/trypsin mixture (1:50, enzyme:protein). Peptides were eluted from the SP3 beads with 2% DMSO. The peptide concentration was measured using the Pierce™ Quantitative Fluorometric Peptide Assay following the manufacturer's instructions. Peptide samples were stored at -20℃ before LC-MS/MS analysis.

LC-MS/MS analysis

All samples were analysed by using an Orbitrap Fusion Tribrid mass spectrometer (Thermo Fisher Scientific), equipped with a Dionex ultra-high-pressure liquid-chromatography system (RSLCnano). Peptides were injected onto a 75 µm × 2 cm PepMap-C18 pre-column and resolved on a 75 µm × 50 cm RP-C18 EASY-Spray temperature-controlled integrated column-emitter (Thermo Fisher Scientific), using a four-hour multistep gradient from 5% B to 35% B with a constant flow rate of 300 nl/min. The mobile phases were: H_2O incorporating 0.1% FA (solvent A) and 80% ACN incorporating 0.1% FA (solvent B).

For total proteome analysis, the data were acquired under the control of Xcalibur software in data-independent acquisition mode (DIA). The survey scan was acquired in the Orbitrap covering the m/z range from 375 to 1,175 Da with a mass resolution of 60,000 and an automatic gain control (AGC) target of 4.0×10^5 ions. MS/MS was performed in the Orbitrap with sequential isolation windows of 10 m/z from 375 to 775 and 40 m/z from 775-1175, with an AGC target of 1.0×10^5 and 60 ms maximum injection time. The fragmentation was performed using a HCD collision energy of 30%.

MS data analysis

For DIA MS analysis, the data from different samples were analyzed using DIA-NN (*45*). The in silico spectral library was generated by DIA-NN from the Homo sapiens database from UniProt (SwissProt October 2021). The FDR threshold was set to 1% for each respective Peptide Spectrum Match (PSM). The data were searched with the following parameters: stable modification of carbamidomethyl (C), variable modifications, acetylation (protein N terminus), with a maximum of 1 missed tryptic cleavage threshold, MBR checked. The MaxLFQ-based protein quantification was performed using an R package, as described previously (*46*).

FIGURES LEGENDS

Figure 1

(A) Study overview. Quality controlled hiPSC lines from 28 donors in their pluripotent state were used for Cell painting and proteomic M/S analysis following addition of 52 FDA approved drugs. 23.2 million cells were imaged across all donors and 871 morphological traits were quantified per donor/drug combination. Variability of drug response of the hiPSC cohort was studied using both phenotypic screening and proteomics.

(B) Heatmap of deviations for each feature from DMSO for each human iPSC line shows variations in the magnitude of drug responses across human iPSC lines. Differential responses to Afatinib, Atorvastatin, Rapamycin and Simvastatin are shown. The response to each drug creates a characteristic pattern of features, but with differences in the magnitude of the response. Color bar shows number of σ from DMSO.

Figure 2

(A) UMAP embedding of cell painting features measured for each hiPSC line used in the study when treated with different drugs. Cell lines are represented on the graph with different shapes and drugs with different colours. Representative separated clusters are indicated by arrows. For visibility, a subset of drugs used in this screen are currently shown.

(B) Induction plot of drug responses for each hiPSC line shows variations in the magnitude of drug responses across hiPSC lines. Variations are plotted as the fraction of features for each combination of drug and hiPSC line that are > 2σ (standard deviation) away from DMSO control.

Figure 3

(A) (B) Volcano plots of proteins showing differential expression in the hiPSC lines stratified by atorvastatin (A) and simvastatin (B) response. Representative proteins that play a role in the HMG-CoA reductase pathway are highlighted in red and show increased expression following atorvastatin and simvastatin treatment.

Figure 4

(A) Volcano plot of proteins showing differential expression in four human iPSC lines stratified by their high or low response to atorvastatin. High response lines: tuju1 and hayt1. Low response lines: denw6 and zaie1. (B) Heat map analysis of proteins

showing differential expression ($|\log_2 FC| > 0.263$) between high and low response hiPSC lines following atorvastatin treatment. StringDB analysis of highly upregulated proteins (>0.2) shown in (B) in high response lines (C) and low response lines (D).

Suppl Figure 1

(A) Maintenance of pluripotency in hiPSC lines in HCS assay format. Representative micrographs from six hiPSC lines plated in 384-well format stained with pluripotency markers (Oct4, Sox2, Nanog and TRA-181). Scale bar; 100µm.

(B) UMAP Embedding of cell painting features measured for eight human iPSC lines from phenotypic screens performed on two different dates (Feb 2022 ("Run #1") and Oct 2022 ("Run #2") on two different imaging systems when treated with different drugs. Cell lines are represented on the graph with different shapes and drugs with different colours. Arrows point to representative drug clusters. Note the reproducibility of the assay results on different dates.

(C) Bar graph of induction values for hiPSC lines treated with atorvastatin and simvastatin. Cell lines used for proteomic analysis are shown in grey boxes.

Suppl Figure 2

(A) Volcano plot of proteins showing differential expression in four hiPSC lines stratified by their high or low response to simvastatin. High response lines: tuju1 and hayt1. Low response lines: denw6 and zaie1. (B) Heat map analysis of proteins showing differential expression ($|\log_2 FC| > 0.263$) between high and low response hiPSC lines following simvastatin treatment. StringDB analysis of highly upregulated proteins ($|\log_2 FC| > 0.263$) shown in the above heat map in high response lines (C) and low response lines (D).

Supplemental Tables

Supplemental Table 1: List of hiPSC lines used in this study

Supplemental Table 2: List of drugs, disease targets and concentrations used in this study

Supplemental Table 3: GO enrichment analysis of top 5% proteins showing increased expression in all four hiPSC lines used for proteomic analysis following atorvastatin treatment. Note pathways related to lipid metabolism.

Supplemental Table 4: GO enrichment analysis of top 5% proteins showing increased expression in all four hiPSC lines used for proteomic analysis following simvastatin treatment.

Supplemental Table 5: GO Enrichment Analysis of gene sets/pathways and their associated p-values for highly expressed proteins (Figure 4 heat map (B) values >0.2) of high response lines following atorvastatin treatment.

Supplemental Table 6: GO Enrichment Analysis of gene sets/pathways and their associated p-values for highly expressed proteins (Figure 4 heat map (B) values >0.2) of low response lines following atorvastatin treatment.

Supplemental Table 7: GO Enrichment Analysis of gene sets/pathways and their associated p-values for highly expressed proteins (Supp Figure 2 heat map (B) values >0.2) of high response lines following simvastatin treatment.

Supplemental Table 8: GO Enrichment Analysis of gene sets/pathways and their associated p-values for highly expressed proteins (Supp Figure 2 heat map (B) values >0.2) of low response lines following simvastatin treatment.

References

1. H. Dowden, J. Munro, Trends in clinical success rates and therapeutic focus. *Nat Rev Drug Discov* **18**, 495-496 (2019).
2. R. K. Harrison, Phase II and phase III failures: 2013-2015. *Nat Rev Drug Discov* **15**, 817-818 (2016).
3. H. T. Rakshith, S. Lohita, A. P. Rebello, P. S. Goudanavar, N. Raghavendra Naveen, Sex differences in drug effects and/or toxicity in oncology. *Curr Res Pharmacol Drug Discov* **4**, 100152 (2023).
4. S. Oh *et al.*, Effectiveness of antipsychotic drugs in schizophrenia: a 10-year retrospective study in a Korean tertiary hospital. *NPJ Schizophr* **6**, 32 (2020).
5. S. Ramkumar, A. Raghunath, S. Raghunath, Statin Therapy: Review of Safety and Potential Side Effects. *Acta Cardiol Sin* **32**, 631-639 (2016).
6. N. D. Wong *et al.*, Residual atherosclerotic cardiovascular disease risk in statin-treated adults: The Multi-Ethnic Study of Atherosclerosis. *J Clin Lipidol* **11**, 1223-1233 (2017).
7. R. J. Tyson *et al.*, Precision Dosing Priority Criteria: Drug, Disease, and Patient Population Variables. *Front Pharmacol* **11**, 420 (2020).
8. K. Takahashi, S. Yamanaka, Induction of pluripotent stem cells from mouse embryonic and adult fibroblast cultures by defined factors. *Cell* **126**, 663-676 (2006).
9. N. Malik, M. S. Rao, A review of the methods for human iPSC derivation. *Methods Mol Biol* **997**, 23-33 (2013).
10. H. Kilpinen *et al.*, Common genetic variation drives molecular heterogeneity in human iPSCs. *Nature* **546**, 370-375 (2017).
11. B. A. Mirauta *et al.*, Population-scale proteome variation in human induced pluripotent stem cells. *Elife* **9**, (2020).
12. K. Takahashi, S. Yamanaka, Induced pluripotent stem cells in medicine and biology. *Development* **140**, 2457-2461 (2013).
13. A. Brenes, Bensaddek, D., Hukelmann, J., Afzal, V. & Lamond, A. I. , The iPSC proteomic compendium. *bioRxiv 469916 (2018) doi:10.1101/469916.*, (2018).
14. M. A. Bray *et al.*, Cell Painting, a high-content image-based assay for morphological profiling using multiplexed fluorescent dyes. *Nat Protoc* **11**, 1757-1774 (2016).
15. C. McQuin *et al.*, CellProfiler 3.0: Next-generation image processing for biology. *PLoS Biol* **16**, e2005970 (2018).
16. L. McInnes, Healy, J. & Melville, J., UMAP: Uniform Manifold Approximation and Projection for Dimension Reduction. . *arXiv [stat.ML]* (2018).
17. E. A. Thomas *et al.*, Antipsychotic drug treatment alters expression of mRNAs encoding lipid metabolism-related proteins. *Mol Psychiatry* **8**, 983-993, 950 (2003).
18. P. Srivastava, D. Panda, Rotenone inhibits mammalian cell proliferation by inhibiting microtubule assembly through tubulin binding. *FEBS J* **274**, 4788-4801 (2007).
19. N. Dogra, A. Kumar, T. Mukhopadhyay, Fenbendazole acts as a moderate microtubule destabilizing agent and causes cancer cell death by modulating multiple cellular pathways. *Sci Rep* **8**, 11926 (2018).
20. P. L. Chari T, The spacious Art of Single-Cell Genomics. *bioRxiv* (2021).

21. C. Willis, J. Nyffeler, J. Harrill, Phenotypic Profiling of Reference Chemicals across Biologically Diverse Cell Types Using the Cell Painting Assay. *SLAS Discov* **25**, 755-769 (2020).
22. T. I. Roumeliotis *et al.*, Genomic Determinants of Protein Abundance Variation in Colorectal Cancer Cells. *Cell Rep* **20**, 2201-2214 (2017).
23. T. Nozue, Lipid Lowering Therapy and Circulating PCSK9 Concentration. *J Atheroscler Thromb* **24**, 895-907 (2017).
24. Y. Huang, R. W. Mahley, Apolipoprotein E: structure and function in lipid metabolism, neurobiology, and Alzheimer's diseases. *Neurobiol Dis* **72 Pt A**, 3-12 (2014).
25. I. F. Tudorache, V. G. Trusca, A. V. Gafencu, Apolipoprotein E - A Multifunctional Protein with Implications in Various Pathologies as a Result of Its Structural Features. *Comput Struct Biotechnol J* **15**, 359-365 (2017).
26. Q. Bi *et al.*, Polymorphisms of the apolipoprotein E gene affect response to atorvastatin therapy in acute ischemic stroke. *Front Cardiovasc Med* **9**, 1024014 (2022).
27. L. Zhang *et al.*, Apolipoprotein E polymorphisms contribute to statin response in Chinese ASCVD patients with dyslipidemia. *Lipids Health Dis* **18**, 129 (2019).
28. C. Cai, Z. Wen, L. Li, The relationship between ApoE gene polymorphism and the efficacy of statins controlling hyperlipidemia. *Am J Transl Res* **13**, 6772-6777 (2021).
29. E. Zintzaras, G. D. Kitsios, F. Triposkiadis, J. Lau, G. Raman, APOE gene polymorphisms and response to statin therapy. *Pharmacogenomics J* **9**, 248-257 (2009).
30. W. J. Shen, S. Azhar, F. B. Kraemer, SR-B1: A Unique Multifunctional Receptor for Cholesterol Influx and Efflux. *Annu Rev Physiol* **80**, 95-116 (2018).
31. R. W. Mahley, Apolipoprotein E: cholesterol transport protein with expanding role in cell biology. *Science* **240**, 622-630 (1988).
32. X. D. Xia *et al.*, Regulation of PCSK9 Expression and Function: Mechanisms and Therapeutic Implications. *Front Cardiovasc Med* **8**, 764038 (2021).
33. E. S. Istvan, J. Deisenhofer, Structural mechanism for statin inhibition of HMG-CoA reductase. *Science* **292**, 1160-1164 (2001).
34. M. S. Brown, J. L. Goldstein, Multivalent feedback regulation of HMG CoA reductase, a control mechanism coordinating isoprenoid synthesis and cell growth. *J Lipid Res* **21**, 505-517 (1980).
35. B. R. Ali, I. Nouvel, K. F. Leung, A. N. Hume, M. C. Seabra, A novel statin-mediated "prenylation block-and-release" assay provides insight into the membrane targeting mechanisms of small GTPases. *Biochem Biophys Res Commun* **397**, 34-41 (2010).
36. E. Ronzier, X. X. Parks, H. Qudsi, C. M. Lopes, Statin-specific inhibition of Rab-GTPase regulates cPKC-mediated IKs internalization. *Sci Rep* **9**, 17747 (2019).
37. S. A. Grunwald *et al.*, Statin-induced myopathic changes in primary human muscle cells and reversal by a prostaglandin F2 alpha analogue. *Sci Rep* **10**, 2158 (2020).
38. B. B. Adhyaru, T. A. Jacobson, Safety and efficacy of statin therapy. *Nat Rev Cardiol* **15**, 757-769 (2018).
39. C. Allan *et al.*, OMERO: flexible, model-driven data management for experimental biology. *Nat Methods* **9**, 245-253 (2012).
40. M. W, Data Structures for Statistical Computing in Python. *Proceedings of the 9th Python in Science Conference* **56-61**, doi:10.25080/Majora-25092bf21922-25000a. (2010).

41. Y. Liao, J. Wang, E. J. Jaehnig, Z. Shi, B. Zhang, WebGestalt 2019: gene set analysis toolkit with revamped UIs and APIs. *Nucleic Acids Res* **47**, W199-W205 (2019).
42. J. Wang, S. Vasaikar, Z. Shi, M. Greer, B. Zhang, WebGestalt 2017: a more comprehensive, powerful, flexible and interactive gene set enrichment analysis toolkit. *Nucleic Acids Res* **45**, W130-W137 (2017).
43. D. Szklarczyk *et al.*, The STRING database in 2023: protein-protein association networks and functional enrichment analyses for any sequenced genome of interest. *Nucleic Acids Res* **51**, D638-D646 (2023).
44. C. S. Hughes *et al.*, Single-pot, solid-phase-enhanced sample preparation for proteomics experiments. *Nat Protoc* **14**, 68-85 (2019).
45. V. Demichev, C. B. Messner, S. I. Vernardis, K. S. Lilley, M. Ralser, DIA-NN: neural networks and interference correction enable deep proteome coverage in high throughput. *Nat Methods* **17**, 41-44 (2020).
46. J. Cox *et al.*, Accurate proteome-wide label-free quantification by delayed normalization and maximal peptide ratio extraction, termed MaxLFQ. *Mol Cell Proteomics* **13**, 2513-2526 (2014).

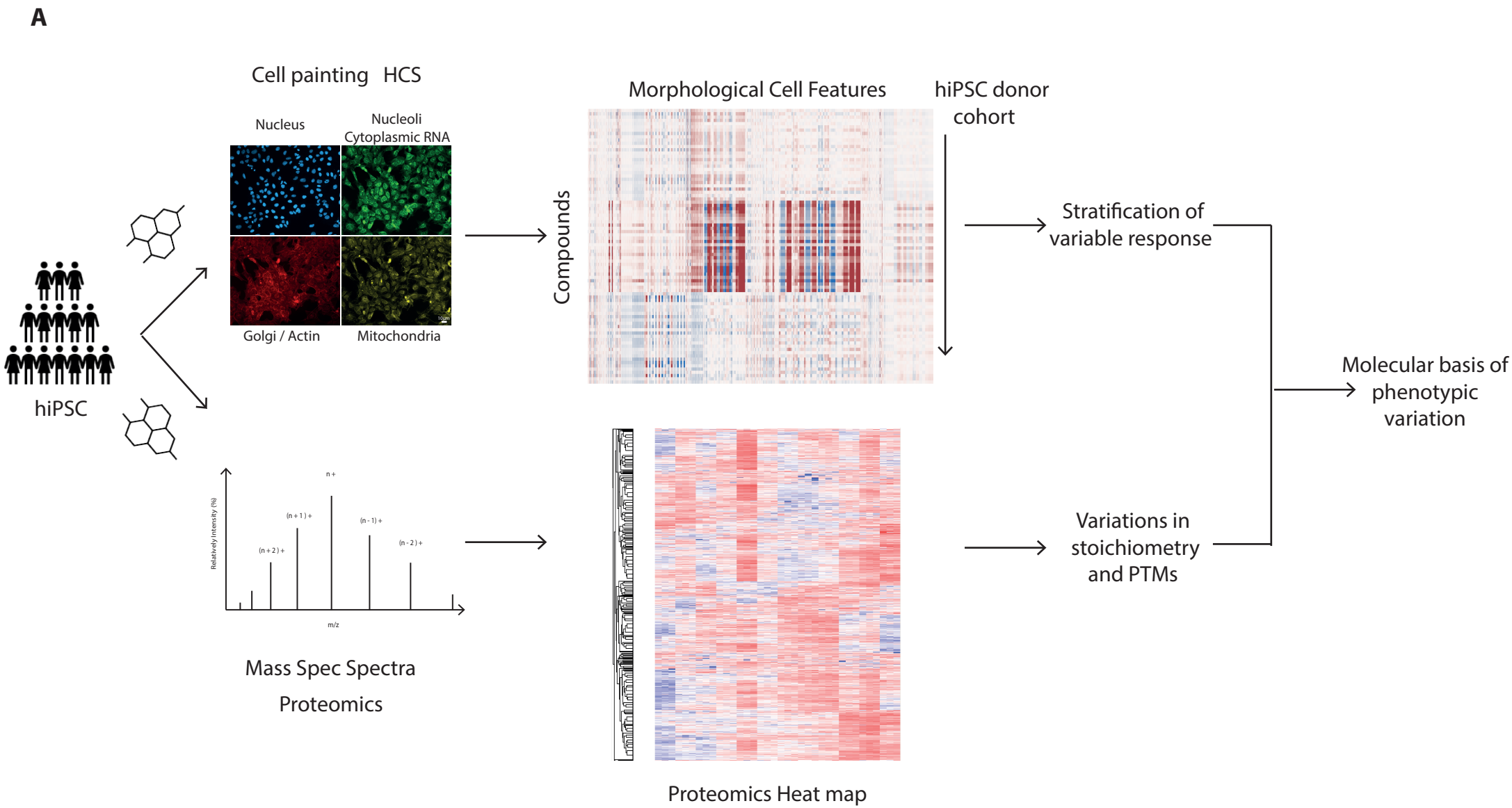
A
Cell painting HCS
Nucleus
Nucleoli
Cytoplasmic RNA
Golgi / Actin
Mitochondria
hiPSC
Compounds
Morphological Cell Features
hiPSC donor
cohort
Stratification of
variable response
Molecular basis of
phenotypic
variation
Relatively Intensity (%)
m/z
Mass Spec Spectra
Proteomics
Proteomics Heat map
Variations in
stoichiometry
and PTMs

Figure 1

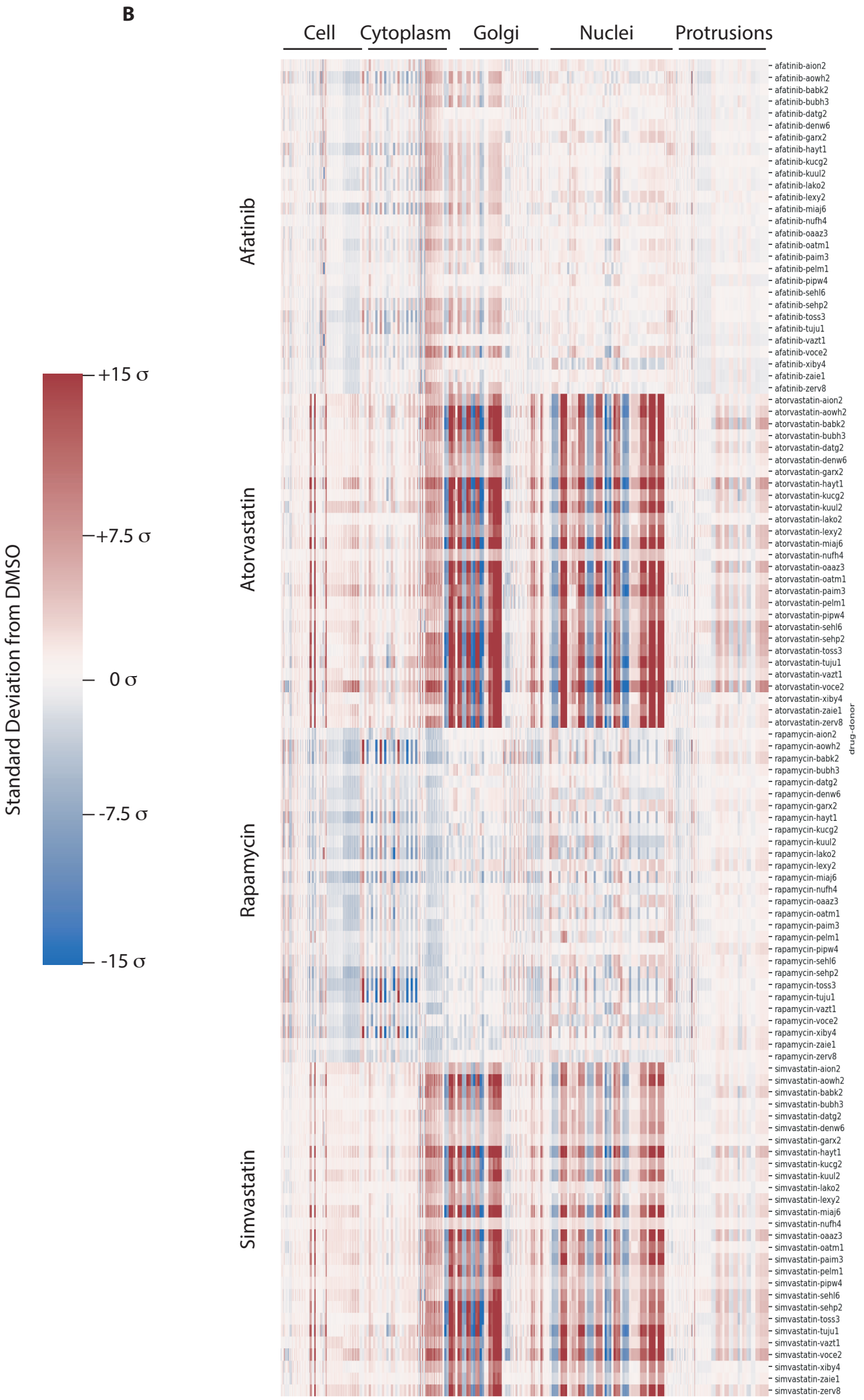
B
Cell
Cytoplasm
Golgi
Nuclei
Protrusions
Afatinib
Atorvastatin
Rapamycin
Simvastatin
afatinib-aion2
afatinib-aowh2
afatinib-babk2
afatinib-bubh3
afatinib-datg2
afatinib-denw6
afatinib-garx2
afatinib-hayt1
afatinib-kucg2
afatinib-kuul2
afatinib-lako2
afatinib-lexy2
afatinib-miaj6
afatinib-nufh4
afatinib-oaaz3
afatinib-oatm1
afatinib-paim3
afatinib-pelm1
afatinib-pipw4
afatinib-sehl6
afatinib-sehp2
afatinib-toss3
afatinib-tuju1
afatinib-vazt1
afatinib-voce2
afatinib-xiby4
afatinib-zaie1
afatinib-zerv8
atorvastatin-aion2
atorvastatin-aowh2
atorvastatin-babk2
atorvastatin-bubh3
atorvastatin-datg2
atorvastatin-denw6
atorvastatin-garx2
atorvastatin-hayt1
atorvastatin-kucg2
atorvastatin-kuul2
atorvastatin-lako2
atorvastatin-lexy2
atorvastatin-miaj6
atorvastatin-nufh4
atorvastatin-oaaz3
atorvastatin-oatm1
atorvastatin-paim3
atorvastatin-pelm1
atorvastatin-pipw4
atorvastatin-sehl6
atorvastatin-sehp2
atorvastatin-toss3
atorvastatin-tuju1
atorvastatin-vazt1
atorvastatin-voce2
atorvastatin-xiby4
atorvastatin-zaie1
atorvastatin-zerv8
rapamycin-aion2
rapamycin-aowh2
rapamycin-babk2
rapamycin-bubh3
rapamycin-datg2
rapamycin-denw6
rapamycin-garx2
rapamycin-hayt1
rapamycin-kucg2
rapamycin-kuul2
rapamycin-lako2
rapamycin-lexy2
rapamycin-miaj6
rapamycin-nufh4
rapamycin-oaaz3
rapamycin-oatm1
rapamycin-paim3
rapamycin-pelm1
rapamycin-pipw4
rapamycin-sehl6
rapamycin-sehp2
rapamycin-toss3
rapamycin-tuju1
rapamycin-vazt1
rapamycin-voce2
rapamycin-xiby4
rapamycin-zaie1
rapamycin-zerv8
simvastatin-aion2
simvastatin-aowh2
simvastatin-babk2
simvastatin-bubh3
simvastatin-datg2
simvastatin-denw6
simvastatin-garx2
simvastatin-hayt1
simvastatin-kucg2
simvastatin-kuul2
simvastatin-lako2
simvastatin-lexy2
simvastatin-miaj6
simvastatin-nufh4
simvastatin-oaaz3
simvastatin-oatm1
simvastatin-paim3
simvastatin-pelm1
simvastatin-pipw4
simvastatin-sehl6
simvastatin-sehp2
simvastatin-toss3
simvastatin-tuju1
simvastatin-vazt1
simvastatin-voce2
simvastatin-xiby4
simvastatin-zaie1
simvastatin-zerv8
drug-donor
hiPSC lines
+15 σ
+7.5 σ
0 σ
-7.5 σ
-15 σ
Standard Deviation from DMSO

Figure 1B

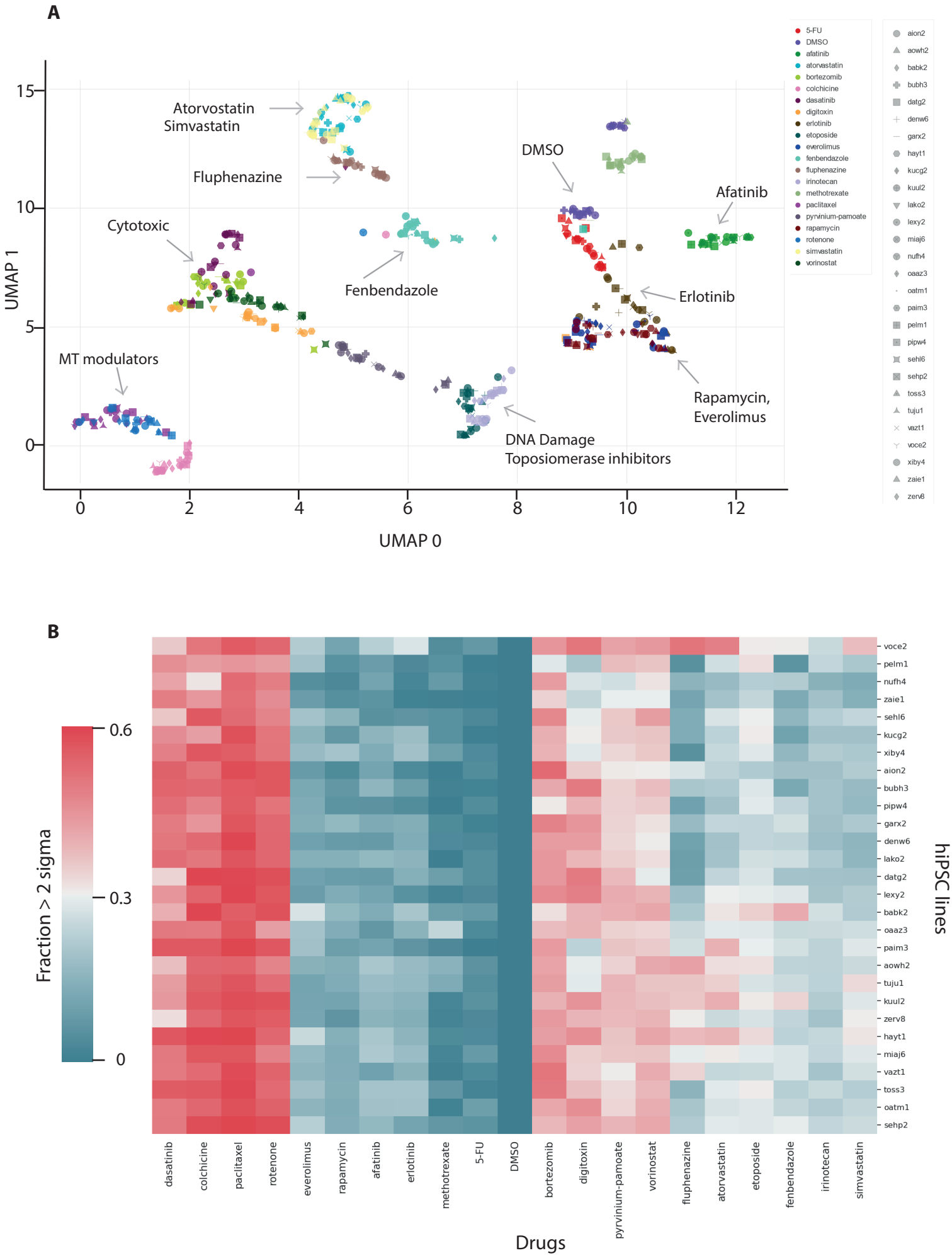
A
Atorvostatin
Simvastatin
Fluphenazine
Cytotoxic
MT modulators
Fenbendazole
DMSO
Afatinib
Erlotinib
Rapamycin,
Everolimus
DNA Damage
Toposiomerase inhibitors
UMAP 1
UMAP 0
5-FU
DMSO
afatinib
atorvastatin
bortezomib
colchicine
dasatinib
digitoxin
erlotinib
etoposide
everolimus
fenbendazole
fluphenazine
irinotecan
methotrexate
paclitaxel
pyrvinium-pamoate
rapamycin
rotenone
simvastatin
vorinostat
B
Fraction > 2 sigma
hiPSC lines
Drugs
dasatinib
colchicine
paclitaxel
rotenone
everolimus
rapamycin
afatinib
erlotinib
methotrexate
5-FU
DMSO
bortezomib
digitoxin
pyrvinium-pamoate
vorinostat
fluphenazine
atorvastatin
etoposide
fenbendazole
irinotecan
simvastatin

Figure 2

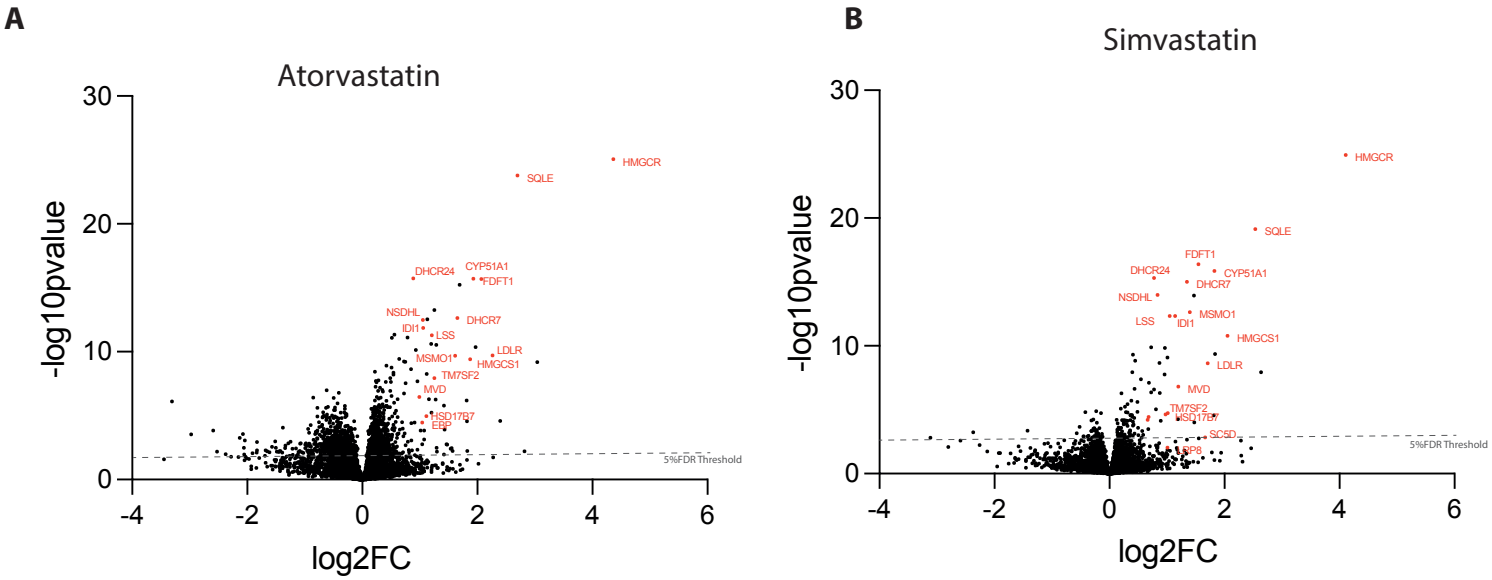
A
Atorvastatin
-log10pvalue
log2FC
HMGCR
SQLE
DHCR24
CYP51A1
FDFT1
NSDHL
DHCR7
IDI1
LSS
LDLR
MSMO1
HMGCS1
TM7SF2
MVD
HSD17B7
EBP
5%FDR Threshold
B
Simvastatin
-log10pvalue
log2FC
HMGCR
SQLE
FDFT1
DHCR24
CYP51A1
DHCR7
NSDHL
MSMO1
LSS
IDI1
HMGCS1
LDLR
MVD
TM7SF2
HSD17B7
SC5D
EBP
5%FDR Threshold

Figure 3

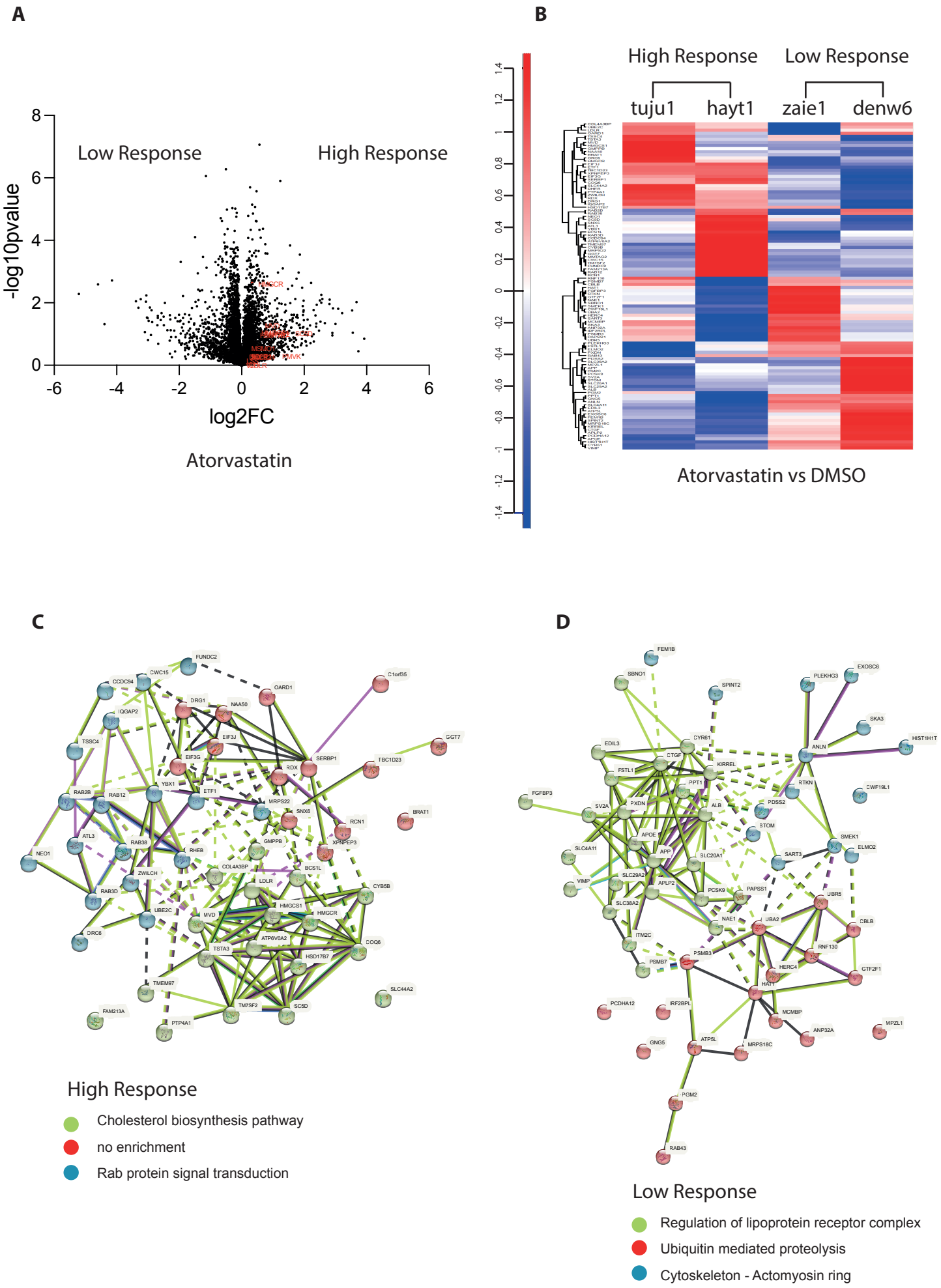
A
Low Response
High Response
-log10pvalue
log2FC
Atorvastatin
B
High Response
Low Response
tuju1
hayt1
zaie1
denw6
Atorvastatin vs DMSO
C
High Response
Cholesterol biosynthesis pathway
no enrichment
Rab protein signal transduction
D
Low Response
Regulation of lipoprotein receptor complex
Ubiquitin mediated proteolysis
Cytoskeleton - Actomyosin ring

Figure 4